Educational Administration: Theory and Practice
2023, 29(4), 3712 -3721
ISSN: 2148-2403
https://kuey.net/ **Research Article**

Artificial Intelligence Power Control Of Integrated Microgrid With Common Dc Link And Power Converter For Improved Efficiency.

Sumalatha Kalakotla[1*], Dr.Cheena Korra[2]

[1*]Research Scholar, Department of Electrical & Electronics Engineering,KU College of Engineering & Technology, Kakatiya University Campus, Warangal, India.
[2]Assistant Professor, Department of Electrical & Electronics Engineering, Uiniversity College of Engineering, Kakatiya University, Bhadradri Kottagudem, India.

Citation: Sumalatha Kalakotla, et.al (2023), Artificial Intelligence Power Control Of Integrated Microgrid With Common Dc Link And Power Converter For Improved Efficiency, *Educational Administration: Theory and Practice*, 29(4), 3712 -3721
Doi: 10.53555/kuey.v29i4.8376

ARTICLE INFO

ABSTRACT

This paper proposes a green energy solution for a microgrid that relies on a diesel generator (DG) to meet its electricity needs. This microgrid is fuelled by two renewable energy sources: wind energy from a doubly fed induction generator (DFIG) and a solar photovoltaic array. The solar PV array is directly connected to the common DC bus of back-back voltage source converters (VSCs) located on the rotor side of the DFIG. Furthermore, a battery energy storage (BES) is coupled to the same DC bus via a bidirectional buck/boost DC-DC converter to provide a path for extra stator power from the DFIG. Rotor side VSC control and bidirectional buck/boost DC-DC converter control are used to harvest the most power from both wind and solar sources. A incremental conductance MPPT algorithm is provided for maximising power from a solar PV array. Furthermore, the regulation of load-side VSC is intended to optimise DG fuel use. A Fuzzy logic concept is utilised to calculate the reference DG power output for the best fuel usage. The microgrid is modelled and simulated using MATLAB's Sim Power Systems toolbox for a variety of scenarios, including shifting wind speeds, varying insolation, the influence of load variation on a bidirectional converter, and an unbalanced nonlinear load connected at the point of common coupling (PCC). The DFIG stator and DG currents are both balanced and sinusoidal.

Keywords: Wind Turbine, doubly fed induction generator (DFIG), diesel generator, solar photovoltaic array, bidirectional buck/boost DC-DC converter, battery energy storage, power quality,Artificial Intelligence (AI).

1. Introduction

A green energy microgrid solution that relies on a diesel generator (DG) to supply its electricity needs is presented in this chapter [1]. Wind energy using a doubly fed induction generator (DFIG) and solar photovoltaic (PV) array are the two renewable energy sources that power this microgrid [2]. The common DC bus of the back-back voltage source converters (VSCs), which are connected in the rotor side of the DFIG, is directly connected to the solar PV array [3]. Additionally, to offer a path for excess stator power of DFIG, a battery energy storage (BES) is connected at the same DC bus via a bidirectional buck/boost DC-DC converter [4]. Bidirectional buck/boost DC-DC converter control and rotor side VSC control are used to maximize the power from both solar and wind, respectively [5]. To maximize power from a solar PV array, a incremental conductance MPPT algorithm is introduced. Additionally, load side VSC regulation is intended to minimize DG's fuel usage [6]. The reference DG power output for optimal fuel economy is calculated using a new idea. The SimPowerSystems toolbox in MATLAB is used to model and simulate the microgrid for a number of scenarios [7], including changing wind speeds, fluctuating insolation, the impact of load fluctuation on a bidirectional converter, and an unbalanced nonlinear load connected at the point of common coupling (PCC) [8]. The DG and DFIG stator currents are found to be sinusoidal and balanced [9]. Figure 1, the microgrid's schematic configuration [10]. It includes linear and nonlinear loads, circuit breakers (CB1 & CB2), ripple filters, DFIG, DG, wind turbine, solar PV array, BES [11], bidirectional buck/boost DC-DC converter, RSC, LSC, interface inductors, Δ/Y transformer [12], and more. For a specific location, this microgrid is intended to provide a maximum load of 50 kW [13].

Each of the solar PV array and wind turbine generator is intended to produce 12.5 kW of power. While the BES is connected via a bidirectional buck/boost DC-DC converter [14], the solar PV array is directly connected to the DC connection in this arrangement. The DG consists of a four-pole synchronous generator [15], a four-stroke reciprocating internal combustion engine, and an automated voltage regulator (AVR) [16]. In accordance with the wind turbine generator's rated capacity, a 25 kVA DG is chosen. As previously said in this research project [17], the design of a wind turbine generator, solar PV array, DG, BES, and other components is completed [18,19].

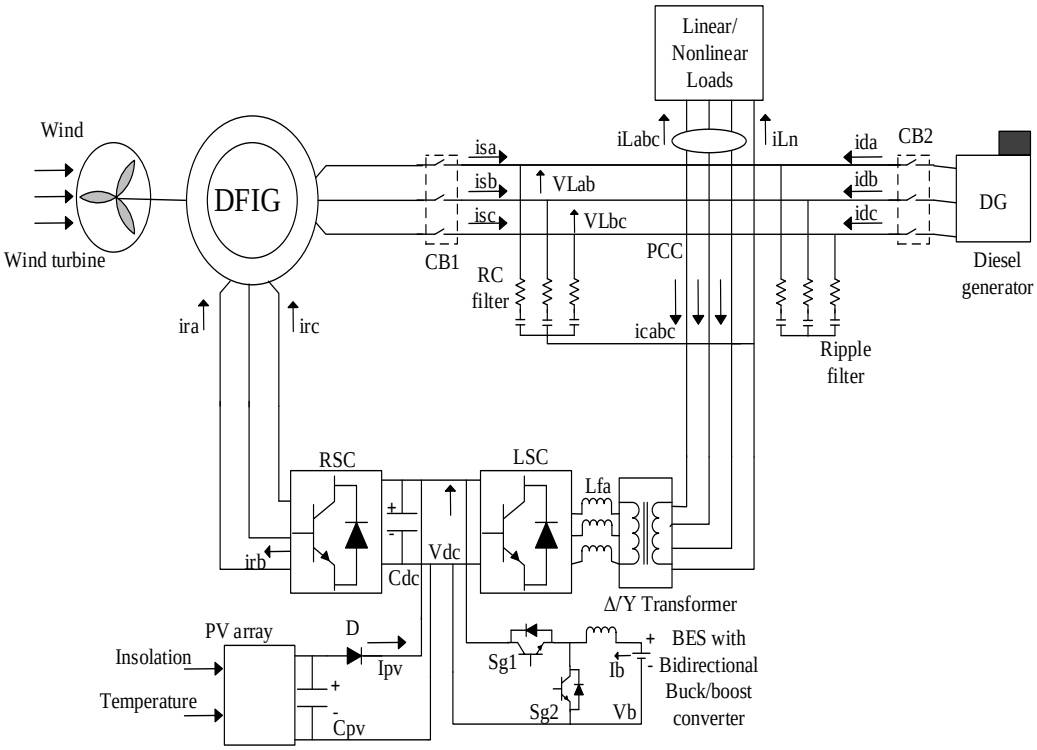

Figure 1: Proposed system Configuration [20].

2. Methodology

In order to reduce the fuel consumption of DG, this work proposes a microgrid based on solar PV array with BES and wind turbine driven DFIG. In this case, a specific household locality's base load requirement is delivered by the DG. The following are the study's primary contributions to the scheme's control aspects.

- In order to maintain the DG's optimal fuel consumption mode, the reference DG power output is calculated using a novel generalized idea.
- Along with power quality concerns like reactive power compensation, load imbalance compensation, and harmonic compensation, the load side converter control (LSC) is made to regulate DG.
- The RSC control is designed to extract maximum power from the wind turbine

A bidirectional buck/boost DC-DC converter connects the BES to the common DC bus of back-back linked VSCs. Its goal is to give DFIG's extra stator power a route. Additionally, a solar PV array is connected to the DC bus directly.

- The bidirectional buck/boost DC-DC converter control is made to manage the current using BES and to maximize the power from the solar PV array.
- A incremental conductance MPPT algorithm is presented to obtain maximum power from a solar PV array.
- Because this microgrid arrangement uses the fewest converters possible, switching losses and overall system costs are decreased.
- The DFIG stator currents and DG currents are maintained balanced and sinusoidal, as per the IEEE 519 standard.
- MATLAB's SimPowerSystems package is used to model and simulate the wind-diesel-solar microgrid with BES. varied wind speeds, varied insolation, the impact on the buck boost converter at different loads, and an unbalanced nonlinear load linked at the point of common coupling (PCC) are all factors that are taken into consideration when analyzing the system performance. Tests are conducted on a created prototype in the lab to verify the microgrid's functionality.

3.Fuzzy Logic Controller (FLC)

This is a modern technology used mostly for the application of power system. FLC implementation is fast and easy, thus preferred for both the system variations (linear and non-linear). In this paper, we used triangular membership functions type for designing inputs and output, which exhibits fast performance and better response even during changes in input variables. FLC processes and fuzzifies the numerical inputs in Fuzzy Inference System (FIS) by applying relevant rules and generates the linguistic output, then defuzzifies the linguistic output back to numerical output during defuzzification process. The translation of fuzzy values is exposed in figures 2a to 2c by membership functions[15].

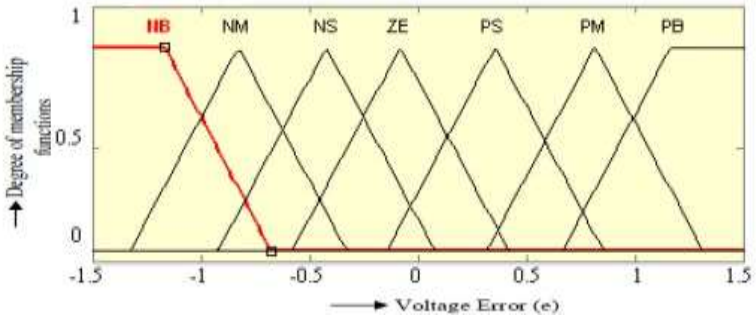

Figure 2a: Membership functions for e[15]

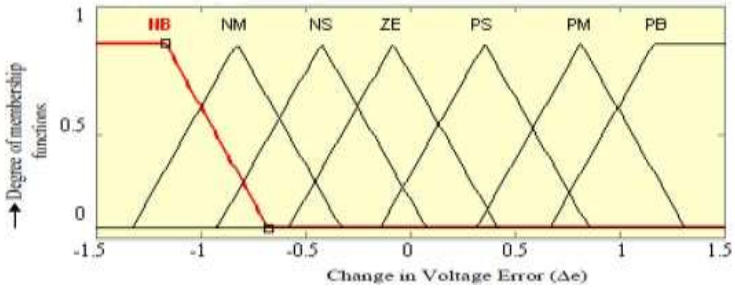

Figure 2b: Membership functions for Δe

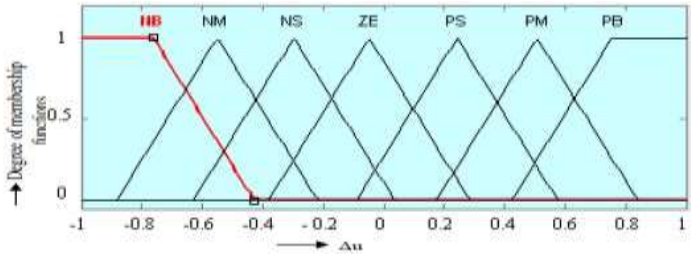

Figure 2c: Membership functions for Δu

The linguistic control rules are stored in the rule base, the rule evaluator uses these rules for decision making and table 1 presents the 49 rules used.

TABLE 1. Rule base of fuzzy controller[15]

Δe/e	NB	NM	NS	ZE	PS	PM	PB
NB	NB	NB	NB	NM	NM	NS	ZE
NM	NB	NB	NM	NS	NS	ZE	PS
NS	NB	NM	NS	NS	ZE	PS	PM
ZE	NM	NS	NS	ZE	PS	PS	PM
PS	NM	NS	ZE	PS	PS	PM	PB
PM	NS	ZE	PS	PS	PM	PB	PB
PB	ZE	PS	PM	PM	PB	PB	PB

The main concentration of this DC link operator is to sustain steady voltage. The evaluation is created for recommendation value and also the actual market value of currents at dc hyperlink and also the error is sent out to FLC operator which moderates the current at dc-link. The FLC controller's result is considered as direct-axis of recommendation present, Id_ref, for the inner current controller.

4. Experimental Procedure and Results Discussion

4.1 Control Methods for Operation of Microgrid

The complete description of control algorithms of RSC and LSC, MPPT algorithm of solar PV array, bidirectional buck/boost DC-DC converter, are given in following subsections.

4.2 Control Algorithm for RSC

The RSC control algorithm is shown in Figure 2. The RSC controls the speed to achieve MPPT from the wind turbine and provides the reactive power needed by DFIG. As illustrated in Fig.3, RSC generates the switching pulses using field oriented vector control (FOVC). Reactive and active components of rotor currents are represented by the FOVC, direct axis, and quadrature axis components (I^*_{dr}, I^*_{qr}), respectively. The no load magnetizing current (Imso) of DFIG is represented by the I^*_{dr}, which is calculated as

$$I_{ms0} = \frac{\sqrt{2}V_L}{\sqrt{3}X_m} \qquad (1)\ [2]$$

where X_m denotes the magnetizing reactance of the machine and V_L is the line voltage at the machine terminals. The I^*_{qr} is estimated by passing the speed error through Artificial Intelligence (AI) controller as depicted in Figure 2 and it is derived as

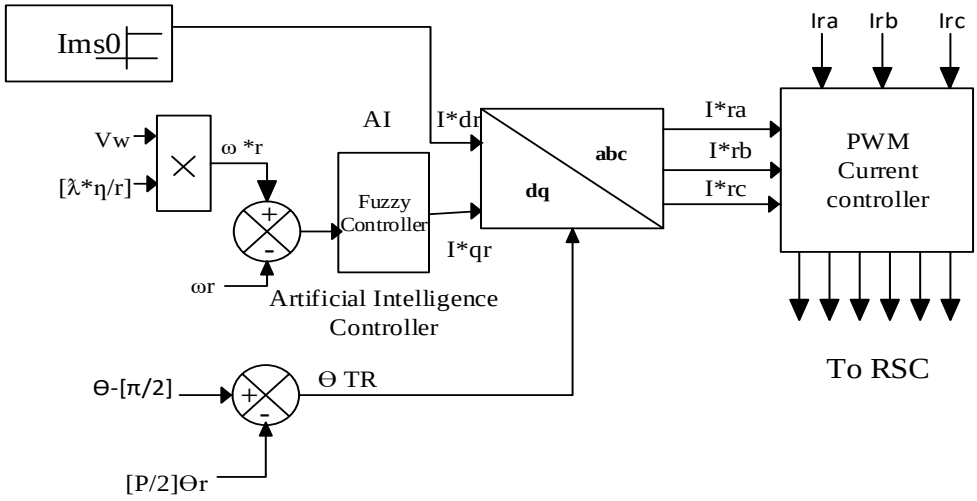

Figure 3. RSC control algorithm

$$I^*_{qr(k)} = I^*_{qr(k-1)} + AI\left(\omega_{err(k)} - \omega_{err(k-1)}\right) + AI\,\omega_{err(k)} \qquad (2)\ [12]$$

where *AI* present Artificial Intelligence contoller constant of speed controller. The $\omega_{err}(k)$ and $\omega_{err}(k\text{-}1)$ denote speed error at *k*th and (*k*-1) th instants, respectively. The $\omega_{err(k)}$, is obtained as

$$\omega_{err(k)} = \omega^*_{r(k)} + \omega_{r(k)} \qquad (3)\ [19]$$

where $\omega^*_{r(k)}$ and $\omega_{r(k)}$ denote the reference and sensed rotor speed of DFIG at kth instant, respectively.
The reference rotor speed is obtained from the tip speed ratio MPPT control as

$$\omega^*_r = \eta\lambda V_w / r$$

Finally, reference rotor currents (i^*_{ra}, i^*_{rb} and i^*_{rc}) are derived from I^*qr and I^*dr using an angle of transformation θ_{TR}, as depicted in figure.3. These reference currents along with sensed rotor currents (i_{ra}, i_{rb} and i_{rc}), are applied to pulse width modulation (PWM) controller to produce RSC gating signals

4.3 Control Algorithm for LSC

The LSC control algorithm is depicted in Figure.3. The LSC is controlled to achieve the following objectives. It maintains the DG and DFIG stator currents sinusoidal and balanced. To attain the best fuel consumption, it controls the DG power between PDmin and PDmax. In order to achieve the best fuel consumption, PDmin and PDmax stand for the minimum and maximum DG power output in pu. The reference currents are produced using a modified indirect vector control based on a voltage-oriented reference frame, as seen in Fig. 5. In order to maximize the power from the DFIG and control the DG power within the range for ideal fuel usage, both DG and DFIG stator currents are added and managed in this.

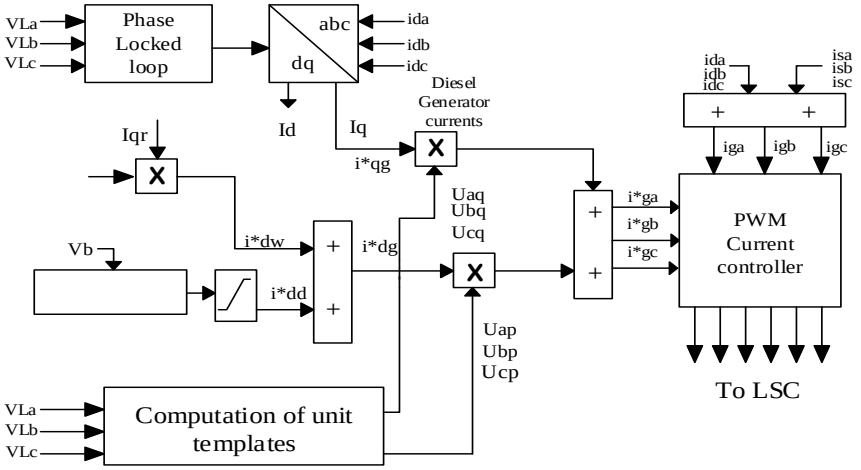

Figure 4. LSC Control Algorithm

4.4 Solar PV Array MPPT Algorithm and Bidirectional Buck/Boost DC-DC Converter Control

By managing power flow through the BES, the bidirectional buck or bidirectional boost DC-DC converter controls the DC link voltage. The solar MPPT is attained in this way. As shown in Figure 4, a incremental conductance MPPT algorithm is employed in this, which entails sampling pulse generation (X) and then estimating the reference DC link voltage (V*dc). The several stages that go into creating the sampling pulse "X" are shown in Figure 4. The sampling pulse is a name in this case.

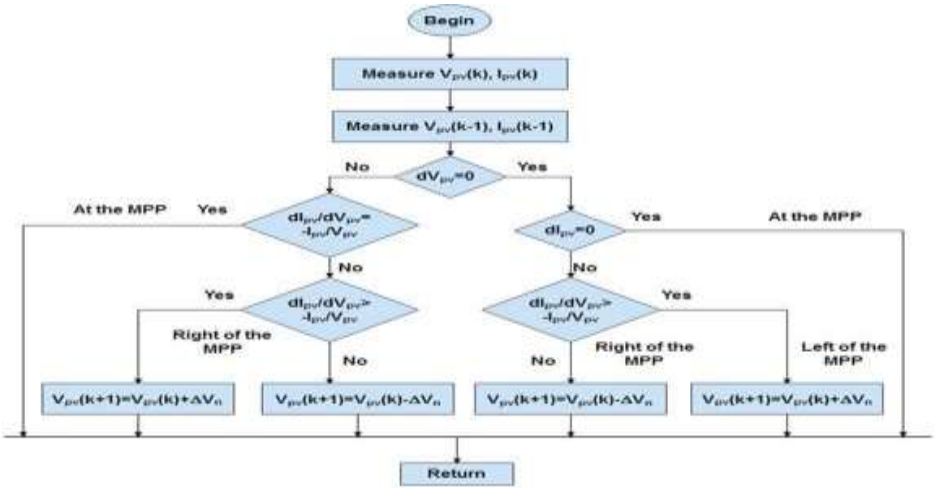

Figure 5 Incremental Conductance algorithmFlowchart

Figure 6 illustrates the bidirectional buck/boost DC-DC converter control. The DC link voltage is controlled by the bidirectional DC-DC boost converter control or the outside artificial intelligence (AI) controller of the bidirectional buck. Furthermore, as shown in Fig. 6, the outer AI controller's output equals the reference battery current (I*b). The reference battery current is monitored by the inner AI controller. Additionally, the duty ratio (R) of the bidirectional buck/boost DC-DC converter is the output of the inner AI controller. The reference battery current (I*b) is derived from Figure 5 as

$$I^*_{b(k)} = I^*_{b(k-1)} = (AI)\left(V_{de(k)} - V_{de(k-1)}\right) + (AI)V_{de(k)}$$

Where, error of the DC link voltage at *k*th instant is

$$V_{de}(k) = V^*_{dc}(k) - V_{dc}(k)$$

Here $V^*_{dc}(k)$ and $V_{dc}(k)$ represent the reference DC link voltage and sensed DC link voltage at k^{th} instant, respectively. *AI* denote the Artificial intelligence controller constants of the outer AI controller

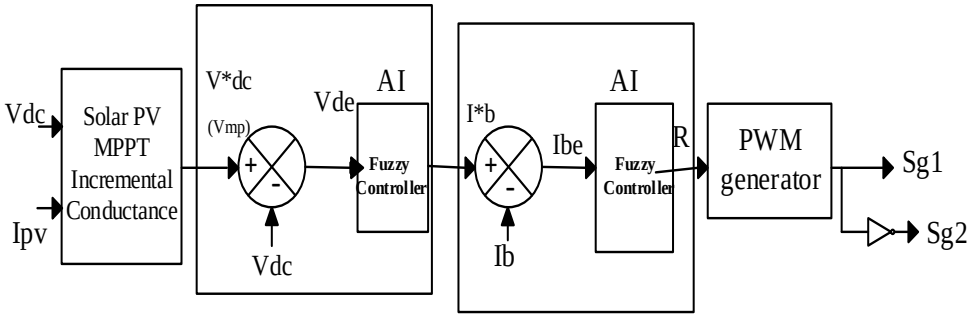

Figure 6 Control of bidirectional buck or bidirectional boost converter

Besides, the duty ratio (*R*) of the bidirectional DC-DC converter, is computed as

$$R_{(k)} = R_{(k-1)} = (AI)\left(I_{be(k)} - I_{be(k-1)}\right) + (AI)I_{be(k)}$$

Where, error of the battery current at *k*th instant is

$I_{be(k)} = I^*_{b(k)} - I_{b(k)}$

Here $I^*_{b(k)}$ and $I_{b(k)}$ represent the reference battery current and sensed battery current at *k*th instant, respectively. Using the determined duty ratio (R), a PWM generator generates pulses for the bidirectional buck or bidirectional boost converter's switches.

4.5 Simulation Results for Validation

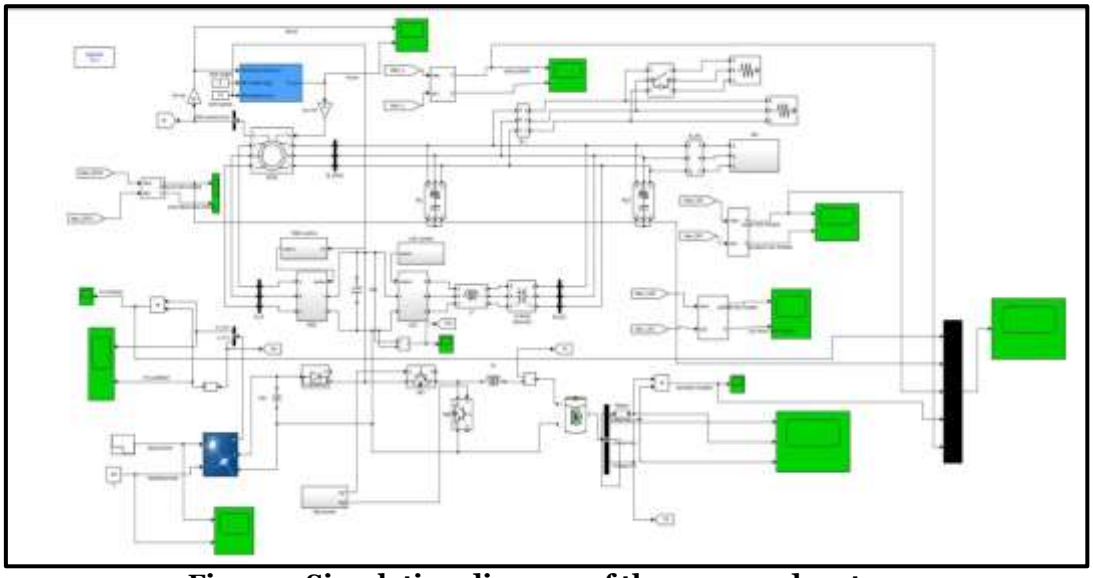

Figure 7 Simulation diagram of the proposed system

The proposed system is modelled in MATLAB and the system parameters are analyszed. PV array is designed to generate an output power of 12.5 kW (peak power) at 300 volts. The following are the PV characteristic considered in this simulation. The Wind Turbine model is taken from the MATLAB library. To The wind turbine the reference speed of 12 m/s and pitch angle 0^0 are given as inputs and the output of the turbine is negative torque which is fed to Asynchronos machine. The DFIG is an asynchronous machine which is taken from the MATLAB simulink. When a negative torque is given to the asynchronous machine it will operate as generator. The stator and rotor are connected to the converters respectively. The two-level converters are considered for as RSC and LSC. The rating of DFIG is 10 kW at 300 voltage. The following are the system parameters. The diesel generator is a synchronous machine taken from the MATLAB library which is designed to delive an ouput power of 25 kW. The load is considered at the PCC. Initial load of 20kW is present with the system and it is increased to 20kW at t= 2 sec, to observe the dynamics of the system. The smulations are shown in the following sector.

i) 0<t<1.5 sec

During this period, the PV power is kept constant as shown in figure 7 and it delivers a power of 11kW at the 300 V. The PV is connected to the DC link terminal which is common for battery RSC and LSC. The PV power is fed

to the grid via the LSC Converter. Diesel generator delivers power of 6kW and DFIG delivers power of 8 kW. The battery is charged in this period as power is available. The following figure shows the power

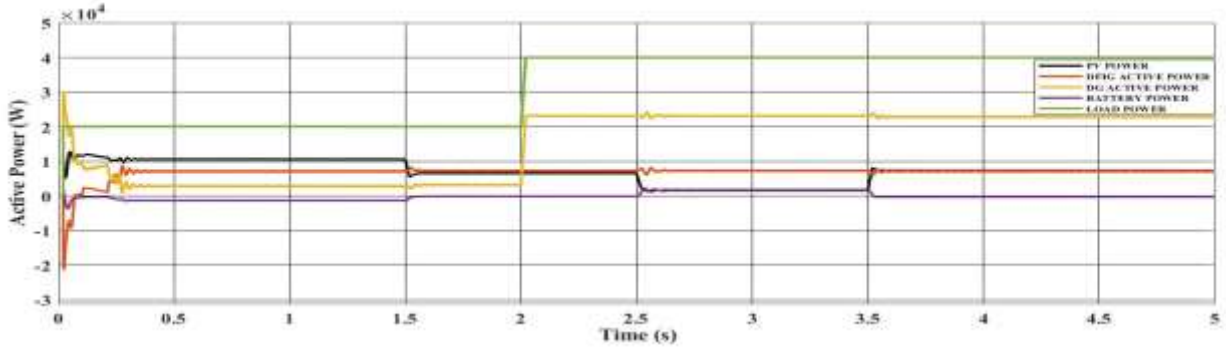

Figure 7 Power waveform of the proposed system

ii) *1.5 sec < t< 2.5 sec*

The PV power is reduced by reducing the Insolation to 500 W/m² at t=1.5 sec which is shown in the figure 8 (a) and (b) The battery which is in charging will now moving towards discharging mode or floating mode as there is no extra power. All the power generated is feeding to the load of 20 kW only. The variation of the power is shown in the below figure. At t = 2 sec, the load is increased to more 20 kW which is shown in the figure 7 and 8 hence a 40 kW is on the system. Corresponding to this increased load, the output power from the diesel generator increases to 25kW as shown in figure 10 and Batter delivers the power of 2 kW which is shown in the figure 12. The wind power is kept constant as there is no change in the wind speed wihcihc shown in the figure 11

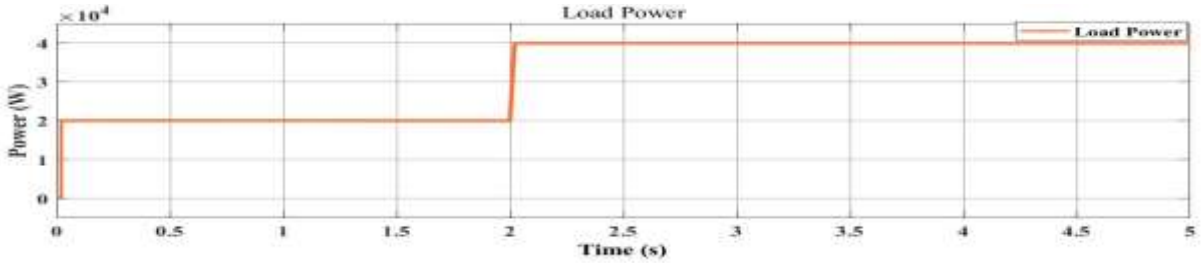

Figure 8 (a) Load Power of the system

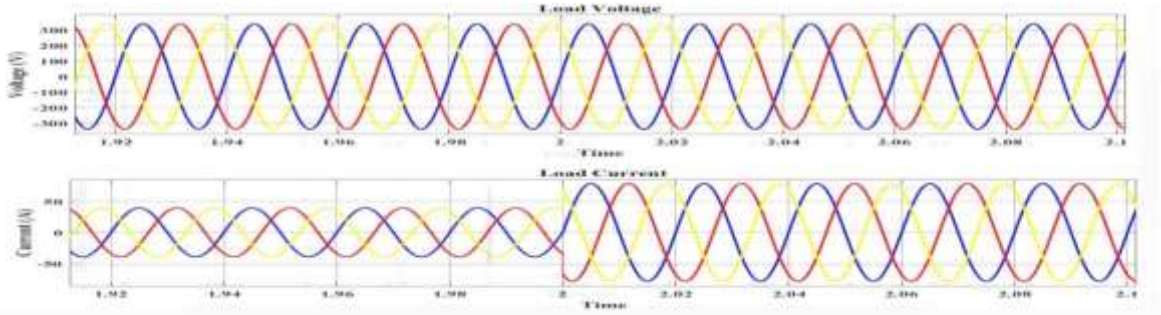

Figure 8 (b) Load Voltage and Current

iii) 2.5 sec < t< 3.5 sec

In this period, the PV power is further reduced, to oberve the battery dynaics. All the power generators have reached their maximum power limit. At t= 2.5 sec, the battery discharges the power and delivers to the load as shown in figure 9 (a) The effect on the diesel generator is reduced because of the battery. Battery is used when during the absence of PV power power. The battery state of charge shows a decline in its characteristics as it is discharged.

iv) t> 3.5 sec

After t= 3.5 seconds, the Insolation is increased to 500 W/m². The battery reduces its power to maintain the system balance which is shown in figure 9 (b), Figure 10 (a), Figure 10 (b), Figure 11, Figure 12 (a) and Figure 12 (b)

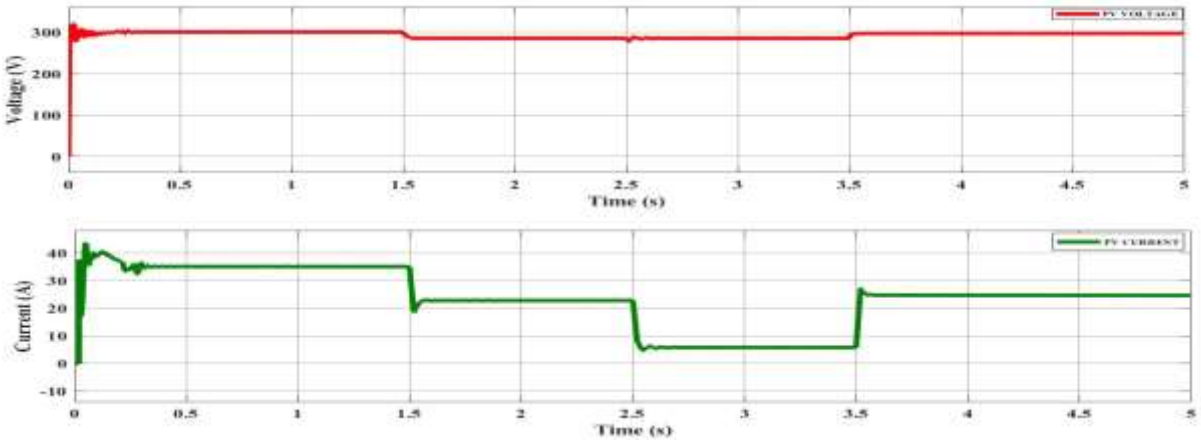

Figure 9 (a) PV voltage and PV Current

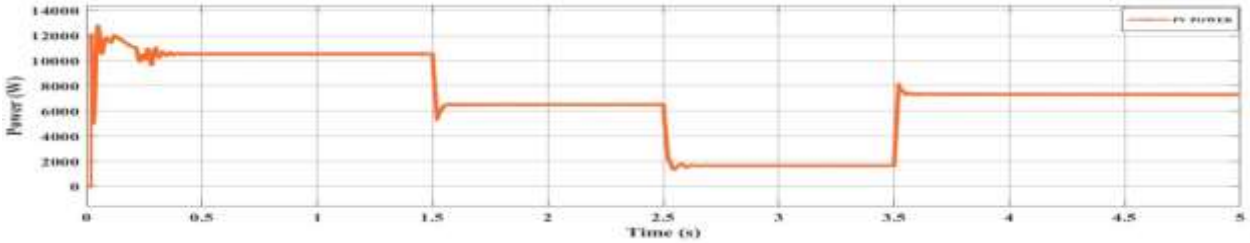

Figure 9 (b) PV Power votlage and current waveforms

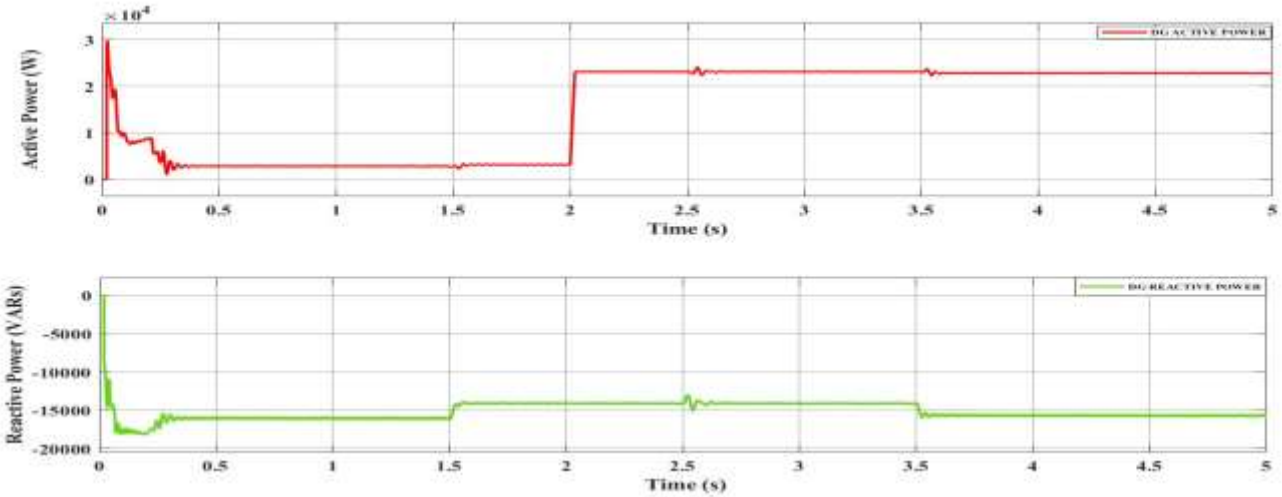

Fig 5.10 (a) Diesel generator Active and Reactive power

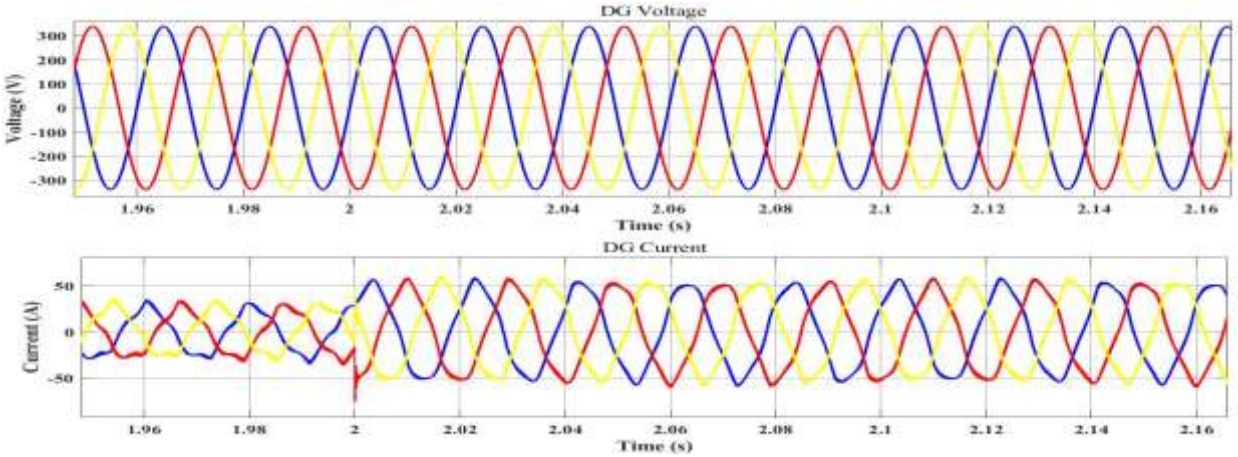

Fig 5.10 (b) Diesel generator votlage and current

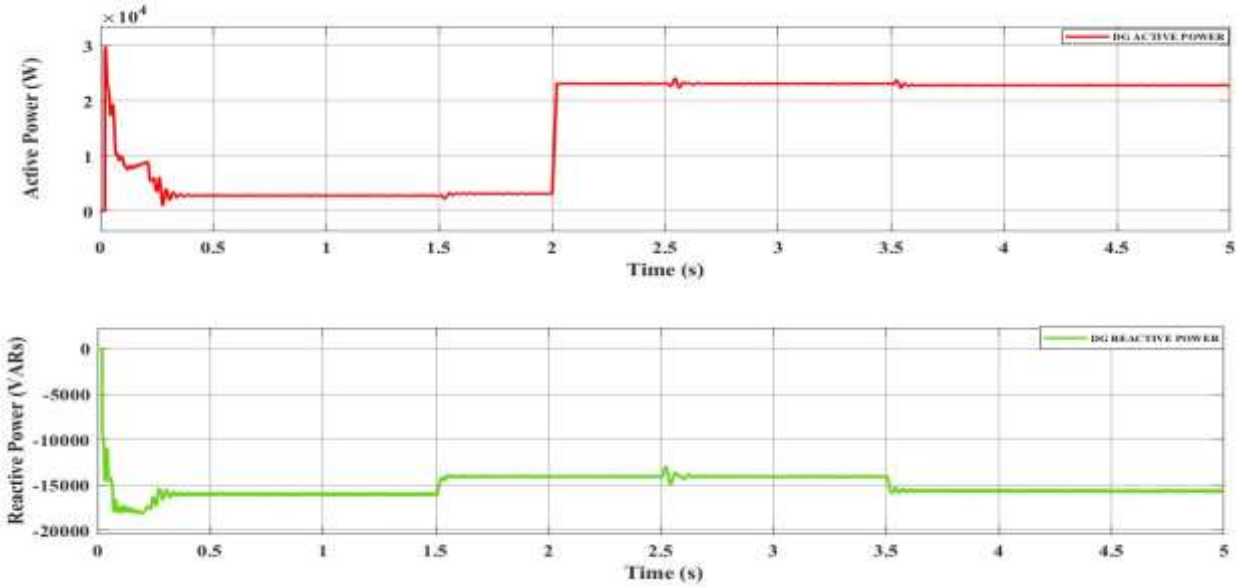

Fig 5.11 DFIG Active and Reactive power

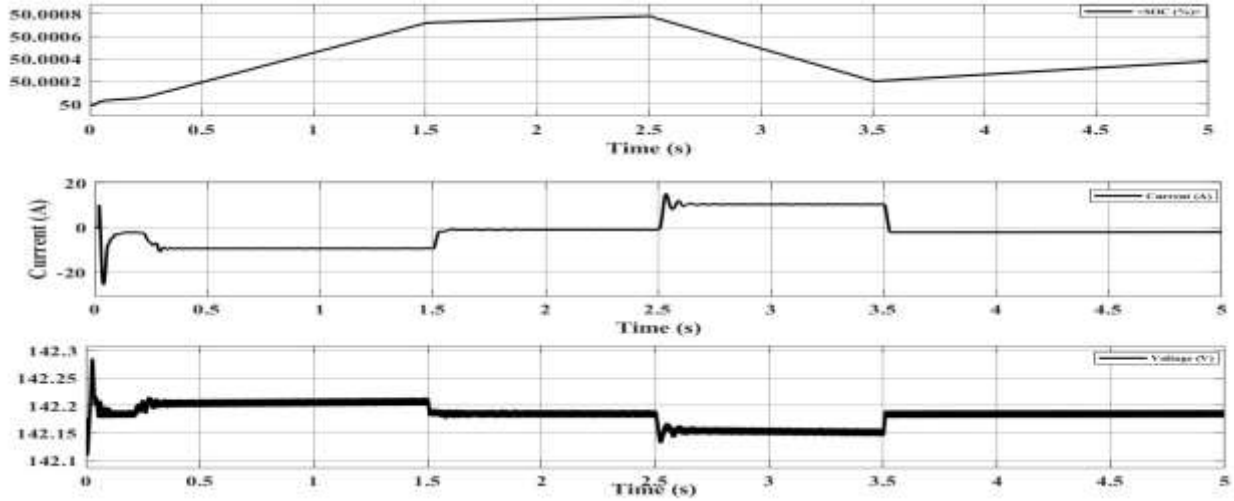

Fig 5.12 (a) Battery parameters: %SOC, Voltage and current

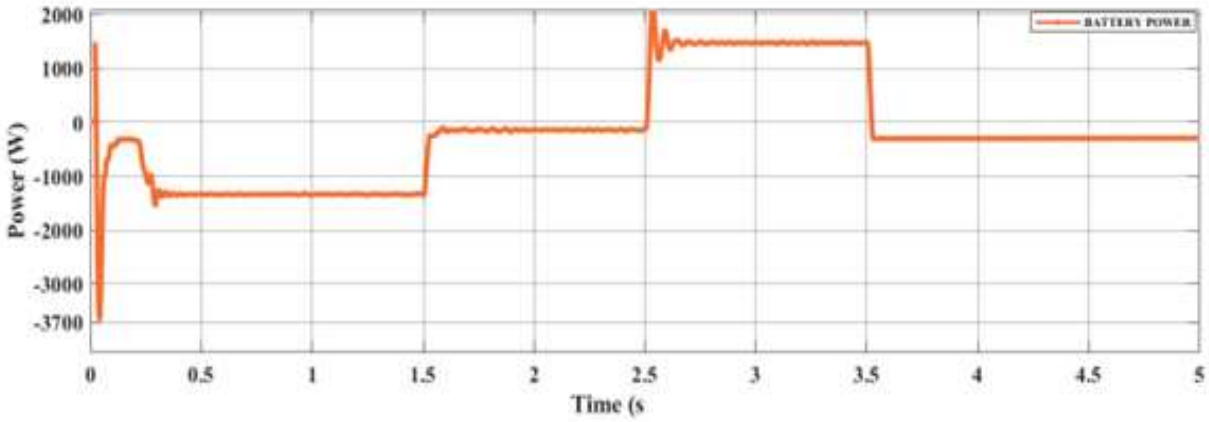

Fig 5.12 (b) Battery power output waveform

5. Conclusion

A microgrid with a minimal number of converters that is powered by wind turbines and consists of DFIG, DG, and solar PV arrays with BES has been introduced. While the BES is connected via a bidirectional buck/boost

DC-DC converter, the solar PV array is directly connected to the DC link of back-back connected VSCs. Numerous scenarios, including variable wind speeds, variable insolation, and an unbalanced nonlinear load linked at PCC, have been studied for the system. Additionally, research has been done on the bidirectional buck/boost DC-DC converter's performance when the load changes. The system's ability to achieve optimal fuel economy has been demonstrated by simulation results. It is discovered that the DG currents, DFIG stator voltages, and currents are balanced.

References

1. A. K. Singh, I. Hussain, and B. Singh, “Double-stage three-phase gridintegrated solar PV system with fast zero attracting normalized least mean fourth based adaptive control,” IEEE Trans. Ind. Electron., vol. 65 , no. 5, pp. 3921-3931, May 2018.
2. T. Adefarati, R. C. Bansal, and J. John Justo, “Techno-economic analysis of a PV–wind–battery–diesel standalone power system in a remote area,” The Journal of Engineering, vol. 2017, no. 13, pp. 740- 744, 2017.
3. N. K. Swami Naidu and B. Singh, “Experimental implementation of doubly fed induction generator-based standalone wind energy conversion system,” IEEE Trans. Ind. Applicat., vol. 52, no. 4, pp. 3332- 3339, July-Aug. 2016.
4. J. Hussain and M. K. Mishra, “Adaptive maximum power point tracking control algorithm for wind energy conversion systems,” IEEE Trans. Energy Convers., vol. 31, no. 2, pp. 697-705, June 2016.
5. N. Nguyen-Hong, H. Nguyen-Duc, and Y. Nakanishi, “Optimal sizing of energy storage devices in isolated wind-diesel systems considering load growth uncertainty,” IEEE Trans. Ind. Applicat., vol. 54, no. 3, pp. 1983-1991, May-June 2018.
6. C. Wu and H. Nian, “Stator harmonic currents suppression for DFIG based on feed-forward regulator under distorted grid voltage,” IEEE Trans. Power Electron., vol. 33, no. 2, pp. 1211-1224, Feb. 2018.
7. J. Knudsen, J. D. Bendtsen, P. Andersen, K. K. Madsen, and C. H. Sterregaard, “Supervisory control implementation on diesel-driven generator sets,” IEEE Trans. Ind. Electron., vol. 65, no. 12, pp. 9698- 9705, Dec. 2018.
8. S. Puchalapalli and B. Singh, “A single input variable FLC for DFIGbased WPGS in standalone mode,” IEEE Trans. Sustainable Energy, vol. 11, no. 2, pp. 595-607, April 2020.
9. W. Li, P. Chao, X. Liang, J. Ma, D. Xu, and X. Jin, “A practical equivalent method for DFIG wind farms,” IEEE Trans. Sustain. Energy, vol. 9, no. 2, pp. 610-620, April 2018.
10. D. Sun, X. Wang, H. Nian, and Z. Q. Zhu, “A sliding-mode direct power control strategy for DFIG under both balanced and unbalanced grid conditions using extended active power,” IEEE Trans. Power Electron., vol. 33, no. 2, pp. 1313-1322, Feb. 2018.
11. S. K. Tiwari, B. Singh, and P. K. Goel, “Control of wind–diesel hybrid system with BESS for optimal operation,” IEEE Trans. Ind. Applicat., vol. 55, no. 2, pp. 1863-1872, March-April 2019.
12. K. Venkatraman, B. Dastagiri Reddy, M. P. Selvan, S. Moorthi, N. Kumaresan, and N. A. Gounden, “Online condition monitoring and power management system for standalone micro-grid using FPGAs,” IET Gener., Trans. & Distr., vol. 10, no. 15, pp. 3875-3884, Nov. 2016.
13. P. Shah, I. Hussain, and B. Singh, “Single-stage SECS interfaced with grid using ISOGI-FLL-based control algorithm,” IEEE Trans. Ind. Applicat., vol. 55, no. 1, pp. 701-711, Jan.-Feb. 2019.
14. J. Jo, H. An, and H. Cha, “Stability improvement of current control by voltage feedforward considering a large synchronous inductance of a diesel generator,” IEEE Trans. Ind. Applicat., vol. 54, no. 5, pp. 5134- 5142, Sept.-Oct. 2018.
15. K. Sumalatha and E. Muneender, "Fuzzy Logic Controller Strategy for Ameliorating DC Link Voltage for Grid Connected Hybrid PV-Wind Generation Systems," 2021 Second International Conference on Smart Technologies in Computing, Electrical and Electronics (ICSTCEE), Bengaluru, India, 2021, pp. 1-7.
16. M. J. Morshed and A. Fekih, “A novel fault ride through scheme for hybrid wind/PV power generation systems,” IEEE Trans. Sustainable Energy, Early Access.
17. Y. Zhang, A. M. Melin, S. M. Djouadi, M. M. Olama and K. Tomsovic, “Provision for guaranteed inertial response in diesel-wind systems via model reference control,” IEEE Trans. Power Systems, vol. 33, no. 6, pp. 6557-6568, Nov. 2018.
18. A. Thakallapelli, S. Kamalasadan, K. M. Muttaqi, and M. T. Hagh, “A synchronization control technique for soft connection of doubly fed induction generator based wind turbines to the power grids,” IEEE Trans. Ind. Applicat., vol. 55, no. 5, pp. 5277-5288, Sept.-Oct. 2019.
19. S. K. Tiwari, B. Singh, and P. K. Goel, “Design and control of autonomous wind–solar system with DFIG feeding 3-phase 4-wire loads,” IEEE Trans. Ind. Applicat., vol. 54, no. 2, pp. 1119-1127, March-April 2018.
20. Y. Zhang, J. Wang, A. Berizzi, and X. Cao, “Life cycle planning of battery energy storage system in off-grid wind–solar–diesel microgrid,” IET Gener., Trans. & Distr., vol. 12, no. 20, pp. 4451-4461, Nov. 2018.
21. Ju Liu, Wei Yao, Jinyu Wen, Jiakun Fang, Lin Jiang, Haibo He, and Shijie Cheng, “Impact of power grid strength and PLL parameters on stability of grid-connected DFIG wind farm,” IEEE Trans. Sustain. Energy, vol. 11, no. 1, pp. 545-557, Jan. 2020.